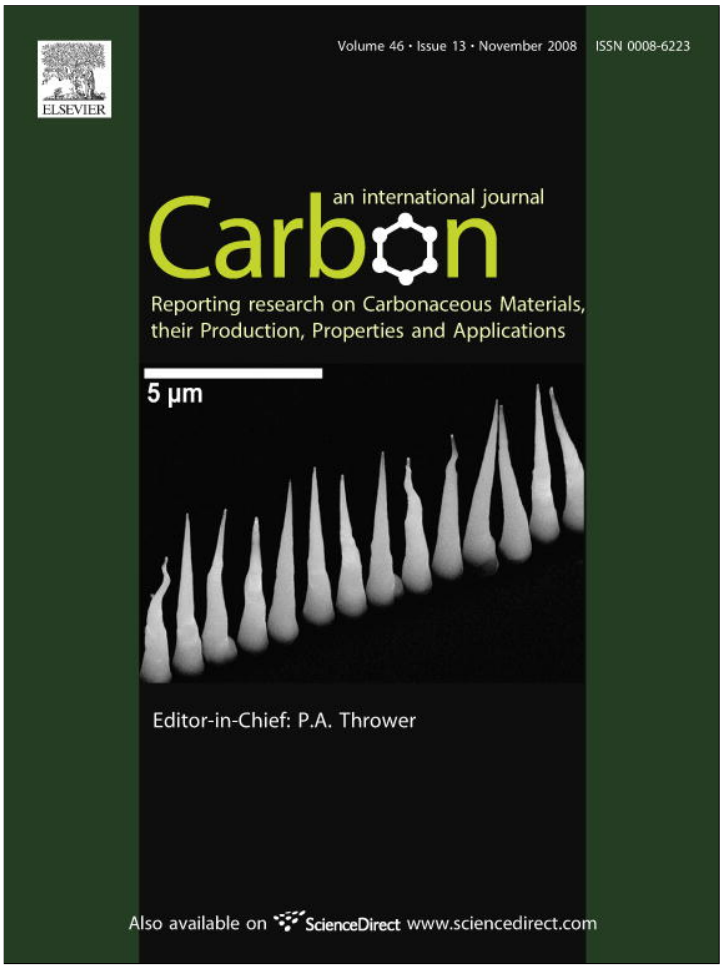

CARBON 46 (2008) 1631–1637

available at www.sciencedirect.com

ScienceDirect

journal homepage: www.elsevier.com/locate/carbon

Synthesis and catalytic application of Pd nanoparticles in graphite oxide

Á. Mastalir[a,*], Z. Király[b], Á. Patzkó[b], I. Dékány[b], P. L'Argentiere[c]

[a]Department of Organic Chemistry, University of Szeged, H-6720 Szeged, Dóm tér 8, Hungary
[b]Department of Colloid Chemistry, University of Szeged, H-6720 Szeged, Aradi vt.1, Hungary
[c]INCAPE, Instituto de Investigaciones en Catálisis y Petroquímica (FIQ-UNL, CONICET), Santiago del Estero, 2654 3000 Santa Fe, Argentina

ARTICLE INFO

Article history:
Received 18 February 2008
Accepted 30 June 2008
Available online 8 July 2008

ABSTRACT

Pd nanoparticles of 1–6 nm were synthesized in graphite oxide (GO) via cation exchange. The synthesis procedure involved immobilization of the precursor $Pd(NH_3)_4(NO_3)_2$ in GO, followed by reduction in flowing H_2. The resulting low-loaded Pd–GO material was characterized by X-ray diffraction (XRD), infrared (IR) spectroscopy and transmission electron microscopy (TEM). Structural characterization revealed that intercalation of the precursor took place in GO and the reduced Pd nanoparticles were situated both on the external surface and in the interlamellar space of the GO lamellae. The catalytic behaviour of Pd–GO was investigated in the liquid-phase hydrogenations of 3-hexyne and 4-octyne under standard conditions. For both reactants, marked turnover frequencies (18–36 s^{-1}) and pronounced (*Z*)-alkene stereoselectivities (93–98.4%) were obtained, indicating that Pd–GO was a highly active and stereoselective catalyst. For the stereoselective hydrogenation of 3-hexyne, Pd–GO exhibited an outstanding catalytic performance: at reactant:Pd (S:Pd) ratios $\leqslant$ 5000, complete conversions were achieved in 8–15 min and the (*Z*)-alkene stereoselectivities exceeded 98%.

1. Introduction

Graphite oxide (GO) is an oxygen-rich carbonaceous material, produced by the controlled oxidation of graphite [1,2]. The structure of GO preserves the hexagonal network of the carbon layers of graphite, but its polyaromatic character is lost, as related to the appearance of oxygen-containing functional groups [3,4]. There are strong covalent bonds within the hexagonal layers of GO and weaker interlayer contacts between intercalated water molecules [5]. The oxygen atoms in GO are bonded to the carbon atoms above and below the carbon layers, in the form of hydroxyl groups and as epoxy bridges, connecting carbon atoms of the same layer. GO also contains a considerable amount of carbonyl and carboxyl groups, located mostly at the sheet edges [6,7]. Several models have been proposed for the structure of GO, including Hofmann's model, in which oxygen atoms are bonded to the hexagonal layers of carbon atoms as epoxy linkages [1,6,8]. More recently, Lerf et al. have suggested a different structure for GO, which contains flat aromatic regions with unoxidized benzene rings and puckered regions of cyclic six-membered rings, bearing enolic, ether, and carboxylic groups [9]. Nevertheless, the nonstoichiometric and strongly hygroscopic character of GO makes its structural elucidation rather difficult [1,10].

Owing to the presence of oxygen-containing polar groups, GO is a hydrophilic material, which readily adsorbs water or other polar liquids [2,7,8]. As a consequence, GO exhibits one-dimensional swelling along the *c* axis, similarly to clay minerals [8]. In slightly basic aqueous solutions, the

* *Corresponding author:* Fax: +36 62 544200.
E-mail address: mastalir@chem.u-szeged.hu (Á. Mastalir).
0008-6223/$ - see front matter
doi:10.1016/j.carbon.2008.06.054

pronounced intracrystalline swelling of GO results in disaggregation, leading to the formation of stable colloidal suspensions [2,4,8,11]. The exfoliation behaviour of GO can be altered by changing its surface properties via chemical functionalization [2,12]. As related to the hydrophilic character, the cation exchange capacity and the intercalation ability of GO, polar organic molecules and polymers can be inserted into its interlamellar space, to form intercalated GO nanocomposites with different basal spacings [5,13]. Such materials can be applied as precursors for the preparation of conductive composites and ultrathin carbon films [7,13]. Further, the application of cationic surfactants with various chain lengths as guest species gave rise to the formation of surfactant-intercalated GO materials, which have been employed as hosts for molecular recognition [5,14,15].

As related to its favourable properties, GO can also be considered as a catalyst support or a host material of catalytically active transition- or noble metal nanoparticles. In the present study, Pd particles have been synthesized in GO via cation exchange. The resulting Pd–GO sample has been characterized and investigated as a catalyst for the liquid-phase hydrogenations of internal alkynes under mild conditions.

2. Experimental

2.1. Synthesis of the Pd–GO sample

GO was prepared from natural graphite flakes (Kropfmühl AG, Germany) according to Brodie's method [16]. For the synthesis of Pd–GO, 1.0 g of finely powdered GO was suspended in 100 cm^3 of distilled water. The pH of the suspension was adjusted to 9 by addition of a 0.1 M NaOH solution. The aqueous suspension of GO was vigorously stirred for 24 h and then filtered by a 500 μm sieve, to eliminate larger particles. The Pd precursor was a 10% $Pd(NH_3)_4(NO_3)_2$ solution (an Aldrich product), for which the pH was adjusted to 10 to eliminate precipitation of the precursor under synthesis conditions. The solution of the precursor (0.2 cm^3) was diluted with distilled water (25 cm^3) and then added dropwise to the GO suspension, followed by an efficient stirring for 3 days. The solid material was subsequently centrifuged, washed with a dilute NaOH solution (pH = 9), distilled water and finally with acetone. The sample was dried in an oven at 333 K overnight. Reduction of the precursor was performed in a 20 cm^3/min H_2 stream at 333 K for 6 h. The Pd–GO sample was stored in a vacuum desiccator until further applications. The Pd content of the solid proved to be 0.18% from ICP-AES analysis.

The adsorption behaviour of Cu(II) amino complexes in diluted aqueous suspensions of GO has been investigated in detail by Kovtyukhova et al. It has been found that the Cu(II) amino complex adsorption was determined by the thickness of the exfoliated GO particles, which depended on the dilution of the suspension [17,18]. Under the experimental conditions of our current study, exfoliation of the GO host did not take place. The concentration of the GO suspension was considerably higher, whereas the initial metal ion concentration was substantially lower than those applied earlier [17,18]. Accordingly, a significantly lower adsorbed metal ion quantity was obtained.

2.2. Characterization

X-ray diffraction patterns were obtained by a Philips PW 1820 diffractometer at 40 kV and 35 mA (CuKα radiation, $\lambda = 0.154$ nm). Before measurement, the samples were dried in an oven at 343 K for 6 h, to remove intercalated water. XRD data were collected in the range $1° < 2\Theta < 30°$ at an interval of 0.01 2Θ. The interplanar spacing d_L was calculated from the first order Bragg reflection by using a PW 1877 automated powder diffraction software.

Infrared spectra were recorded by a Bio-rad Digilab Division FTS-65A/896 spectrometer, equipped with a DTGS detector, in the range 400–4000 cm^{-1}, by applying an optical resolution of 4 cm^{-1}. The samples were investigated as Nujol mulls. The spectrum of Nujol has been carefully subtracted from those of the samples after measurement.

TEM investigations were performed by a Philips C10 transmission electron microscope (LaB_6 cathode, 100 kV) equipped with a Megaview II digital camera. The samples were dispersed in ethanol and mounted on a Formvar-coated copper grid, followed by solvent evaporation. The size distribution of the Pd particles and the mean crystallite diameter ($d = \Sigma n_i d_i / \Sigma ni$) were determined from several images, for at least 200 particles, by using AnalySIS 3.1. software.

2.3. Catalytic test reaction

The catalytic behaviour of the Pd–GO sample was investigated in an automated vibration reactor [19], for the liquid-phase hydrogenations of 3-hexyne and 4-octyne (both Aldrich products of 99% purity) under standard conditions (298 K, 10^5 Pa). The mass of catalyst was 5 mg and the reactant:Pd ratio (S:Pd) was varied between 2500 and 10,000. Pretreatment of the sample was effected in 10^5 Pa of static H_2 for 60 min, followed by evacuation. After reintroduction of H_2, 1 cm^3 of toluene was added as a dispersion medium and pretreatment was completed under vigorous stirring for 45 min. The catalytic reactions were carried out under efficient stirring (1400 rpm) in order to eliminate mass transport limitations. As the reactions progressed, the H_2 consumption was monitored at a data collection frequency of 0.5 s^{-1}. The initial rates were determined from the slopes and the turnover frequencies (TOF) were calculated. The product mixtures were analyzed by a HP 5890 gas chromatograph equipped with a DB-1 capillary column and a flame ionization detector (FID). The catalytic runs were repeated up to 3 times, the results displayed a standard deviation of ±2.6%.

For comparative investigations, 1% Pd/C (an Aldrich product) and 1% Pd/graphimet (an Alfa product) were utilized. The Pd dispersions D of the samples were determined from TEM measurements as $D = 0.885/d$, where d is the mean particle diameter (nm) [20]. The dispersion values obtained were 0.17 and 0.25 for Pd/C and Pd/graphimet, respectively [21].

3. Results and discussion

The XRD pattern of the ion exchanged sample $Pd(NH_3)_4$–GO was found to be the same as that obtained for the reduced sample Pd–GO. The X-ray diffractograms of pristine GO and

Pd–GO are demonstrated in Fig. 1. For the air-dried GO material, a well-defined peak was obtained at $2\Theta = 12.9°$, which corresponds to an interplanar distance (d_L) of 0.69 nm. It may be observed in Fig. 1 that drying at 343 K for 6 h considerably decreased the interlamellar water content of GO, as revealed by the shift of the characteristic reflection towards higher angles and also by its enhanced intensity. Accordingly, the basal spacing of dried GO proved to be 0.63 nm. This finding complies with the results of Lerf et al., who have established a strong variation of the layer distances of GO as a function of their intercalated water content [11].

The absence of the characteristic d_{002} reflection of graphite at 26.6° gave evidence that complete oxidation was achieved [10], leading to the formation of a well-ordered, lamellar structure, which is more open than that of graphite ($d_L = 0.336$ nm) and thus more susceptible to intercalation [10]. For the XRD pattern of Pd–GO, the characteristic peak of GO could be no longer observed, indicating that a significant structural change occurred upon immobilization of the Pd particles. The appearance of peaks at lower diffraction angles signifies increased basal spacings (1.19 nm and 3.35 nm), which may be attributed to intercalation of the Pd particles in the interlayer space of GO. Both d_L values are significantly higher than that of pristine GO, indicating that the lamellae moved apart. The enhanced basal spacing is anticipated to exert a favourable effect on the catalytic behaviour of the Pd–GO sample.

The infrared spectra of the complex precursor $Pd(NH_3)_4(NO_3)_2$, the ion exchanged sample $Pd(NH_3)_4$–GO and the reduced Pd–GO material are demonstrated in Figs. 2 and 3. For the precursor $Pd(NH_3)_4(NO_3)_2$, the bands at 3300 cm^{-1} and 3200 cm^{-1} correspond to the symmetric υ_s-(NH_3) and antisymmetric υ_{as}-(NH_3) modes, respectively (Fig. 2). These bands no longer appear for Pd–GO, which signifies that complete reduction was achieved. However, the above bands can be clearly distinguished for the $Pd(NH_3)_4$–GO sample, which confirms that the complex precursor was immobilized in GO.

The position of the υ_s-(NH_3) band did not alter significantly, whereas the υ_{as}-(NH_3) band was shifted towards higher wavenumbers, indicating a weaker Pd–NH_3 interaction than that in the original precursor. This implies that the character of the Pd–N bond was altered upon immobilization in GO: the distances between the Pd^{2+} cation and the NH_3 ligands were increased, which may be attributed to the effect of the GO host.

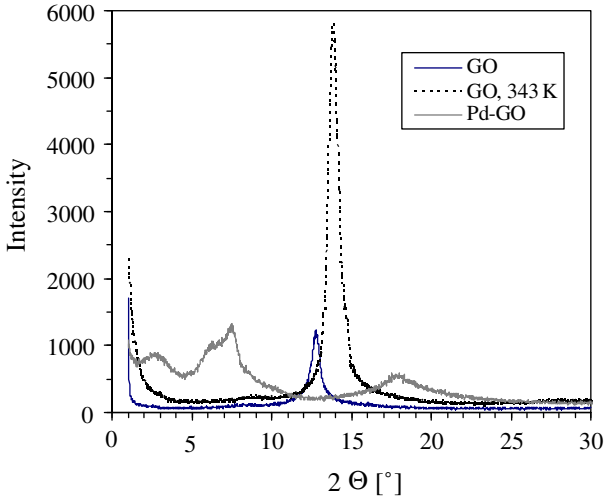

Fig. 1 – XRD patterns of GO and Pd–GO.

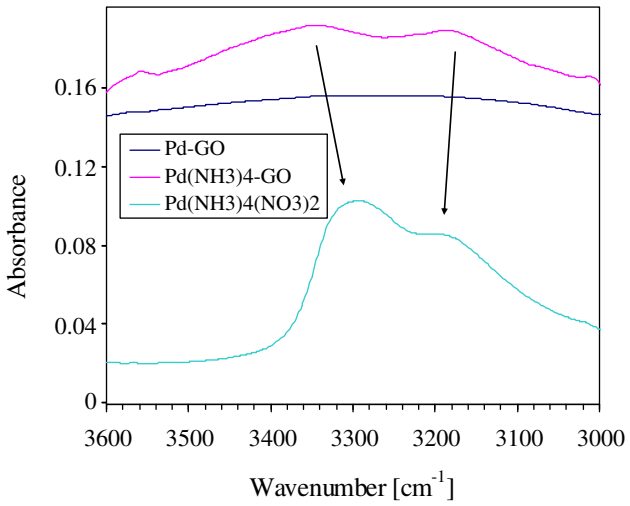

Fig. 2 – Infrared spectra of the precursor $(Pd(NH_3)_4(NO_3)_2$, ion-exchanged GO ($Pd(NH_3)_4$–GO) and ion-exchanged GO after reduction (Pd–GO), in the range 3000–3600 cm^{-1}.

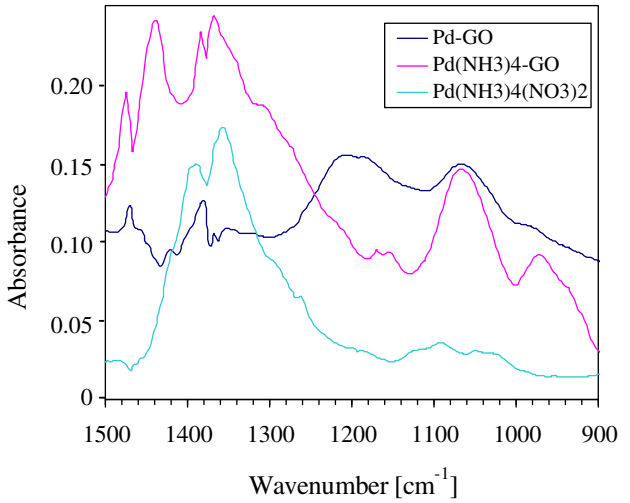

Fig. 3 – Infrared spectra of the precursor $(Pd(NH_3)_4(NO_3)_2$, ion-exchanged GO ($Pd(NH_3)_4$–GO) and ion-exchanged GO after reduction (Pd–GO), in the range 900–1500 cm^{-1}.

In Fig. 3, the band at 1354 cm^{-1}, which is characteristic of the $Pd(NH_3)_4(NO_3)_2$ complex precursor, appears in the spectrum of $Pd(NH_3)_4$–GO material at 1371 cm^{-1}, but cannot be observed in that of the reduced Pd–GO sample. The band shift towards higher wavenumbers can also be assigned to the effect of the GO host material, which represents a different chemical environment from that in the complex precursor. Accordingly, Fig. 3 clearly indicates the immobilization of $Pd(NH_3)_4^{2+}$ cations in GO and also a modification of the Pd^{2+}–ligand interaction.

As the characteristic bands of free ammonia could not be identified for $Pd(NH_3)_4$–GO, it follows that ammonia ligands

were not released from the complex precursor upon immobilization. However, the infrared spectra gave evidence that the ammonia ligands in the $Pd(NH_3)_4$–GO sample were more weakly bound to the Pd^{2+} cation than those in the complex precursor. This may be related to the formation of electrostatic interactions between the intercalated $Pd(NH_3)^{2+}$ cations and the negatively charged functional groups of the GO host. According to the above considerations, the variation in the basal spacings of both $Pd(NH_3)_4$–GO and Pd–GO may be attributed to different orientations of the guest species [14]. It is reasonable to assume that d_L = 1.19 nm is related to the intercalated $Pd(NH_3)_4^{2+}$ cations situated parallel to the surface of GO, whereas the enhanced value of d_L = 3.35 nm originates from a perpendicular orientation [14]. The different arrangements of the complex cations may be assigned to the heterogeneous distribution of the negatively charged surface sites of the GO host [4]. Closely-spaced cation exchange positions favour a perpendicular arrangement of the guest species, whereas loosely-spaced positions favour a parallel orientation.

Figs. 4a and b display the transmission electron micrographs of GO and Pd–GO. In Fig. 4a, the lamellar structure of pristine GO can be clearly distinguished, which resembles those of clay minerals [22].

The TEM image of Pd–GO is shown in Fig. 4b. It may be observed that most of the Pd particles were decorating the edges of the GO lamellae. As compared with supported metal catalysts, a rather limited number of Pd particles were detected on the external surface, which suggests that some of the particles are intercalated between the GO lamellae. This is also reinforced by the appearance of spherical particles with low contrasts, typical of intercalated or embedded particles. The particle size distribution is illustrated in Fig. 5.

It may be observed in Fig. 5 that a major proportion of the particles (77%) fell in the narrow range 2–4 nm, whereas crystallites smaller than 2 nm and larger than 5 nm occurred far less frequently. Aggregates larger than 6 nm were not detected. Particle size analysis indicated that the mean crystallite diameter d was 3.54 nm. From this value, the dispersion of the Pd particles was calculated as $D = 0.885/d$ [20] and proved to be 25%. The results of TEM measurements gave evidence that the particle diameters were comparable with the enhanced basal spacing of Pd–GO (3.35 nm), determined by XRD. By considering the lower value of d_L = 1.19 nm, it may

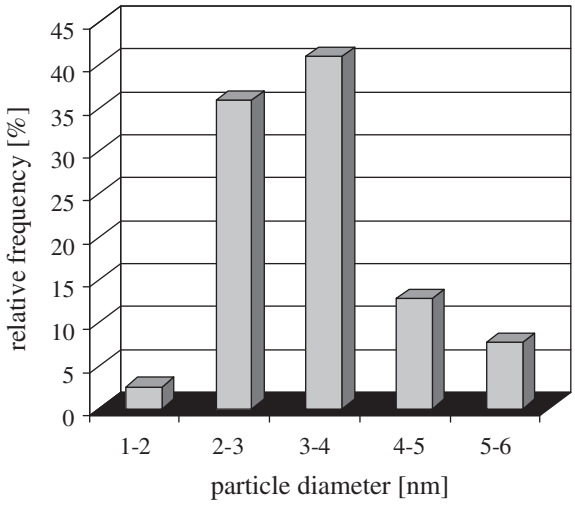

Fig. 5 – Particle size distribution of Pd–GO.

be assumed that particles smaller than 1 nm were also formed in the interlamellar region, although such particles were not detected on the external surface of Pd–GO.

For hydrogenation reactions, catalytic activity is considered to be a function of both electronic and geometric factors associated with the active sites, which are fully reduced metal crystallites. Of all transition metals, Pd offers the most favourable combination of activity and selectivity and therefore it has become the basis of the most efficient alkyne hydrogenation catalysts developed for the synthesis of fine chemicals [23]. Accordingly, the catalytic performance of the Pd–GO sample was investigated for the selective hydrogenations of the internal alkynes 3-hexyne and 4-octyne (Fig. 6) under mild conditions.

The major product of the hydrogenation of internal alkynes is the (Z)-alkene stereoisomer, which is attributed to the associative adsorption of the reactant on the active sites [24]. The (Z) product is typically formed by the consecutive addition of two adsorbed hydrogen atoms from below the axis of the double bond. In contrast, the reaction of molecular hydrogen results in the formation of the (E)-alkene [24,25]. The stereoselectivity of (Z)-alkene formation is based on a kinetic factor if the reaction rates of subsequent reactions are lower than that of partial hydrogenation. Further, the

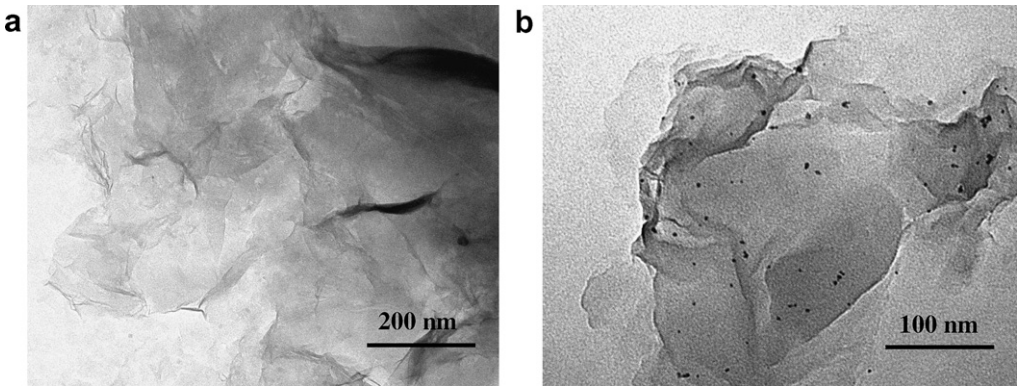

Fig. 4 – (a and b) TEM images of GO and Pd–GO.

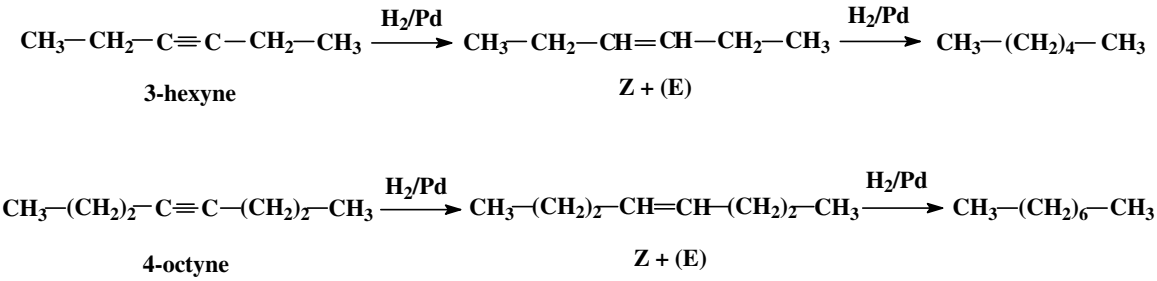

Fig. 6 – Catalytic hydrogenations of 3-hexyne and 4-octyne.

electrophilic character of the triple bond ensures that it is more strongly adsorbed on the active sites than the corresponding double bond [26]. Accordingly, the alkyne reactant either displaces the primarily formed alkene from the surface of the catalyst or blocks its readsorption [26,27]. Hence, the alkyne acts as a catalyst poison for additional reactions, which results in a thermodynamically dependent selectivity. Kinetic and thermodynamic effects are frequently combined and cannot be readily distinguished [26].

As displayed in Fig. 7, the H_2 consumption obtained for the reaction of 3-hexyne over Pd–GO corresponds to a typical zero order reaction, which is characteristic of alkene and alkyne hydrogenations over supported metal catalysts [28,29]. Irrespective of the S:Pd ratio, the initial rate was maintained as the reaction progressed, indicating that the active centres were readily accessible for the reactant molecules [30]. On the other hand, for the transformation of 4-octyne, the H_2 consumption exhibited a completely different trend, as shown in Fig. 8.

After a short induction period, hydrogenation started with a high initial rate, which declined rapidly after a few minutes and then the reaction slowed down considerably. The plots displayed in Fig. 6 belong to different S:Pd ratios. For an enhanced S:Pd ratio of 5000, a loss in the reaction rate was observed after a shorter reaction time than that for S:Pd = 2500. The decrease in the hydrogenation rate may be attributed to the presence of interlamellar Pd particles, which participate in the reactions as active sites and appear to be less accessible for the 4-octyne molecules than those on the external surface of the catalyst [19]. As a consequence, the hydrogenation rate tends to be controlled by transport phenomena as the reaction proceeds [31]. It follows that interlamellar Pd particles participate in the reactions as active centres, whereas the role of external surface crystallites is less significant. This finding is in accordance with the results of XRD and TEM measurements. It may therefore be established that the catalytic behaviour of Pd–GO is essentially different from those of conventional supported Pd catalysts. The linear trend obtained for the hydrogenation rate of 3-hexyne can be explained by considering that, being a smaller molecule than 4-octyne, 3-hexyne can enter the interlamellar region of the GO host. The data obtained for the hydrogenations of internal alkynes are summarized in Table 1.

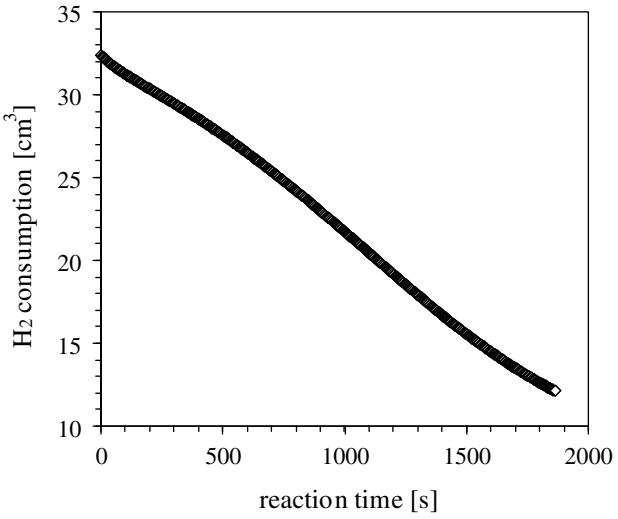

Fig. 7 – Hydrogenation of 3-hexyne over Pd–GO $m = 5 \times 10^{-5}$ g, $T = 298$ K, $p = 10^5$ Pa, S:Pd = 10,000.

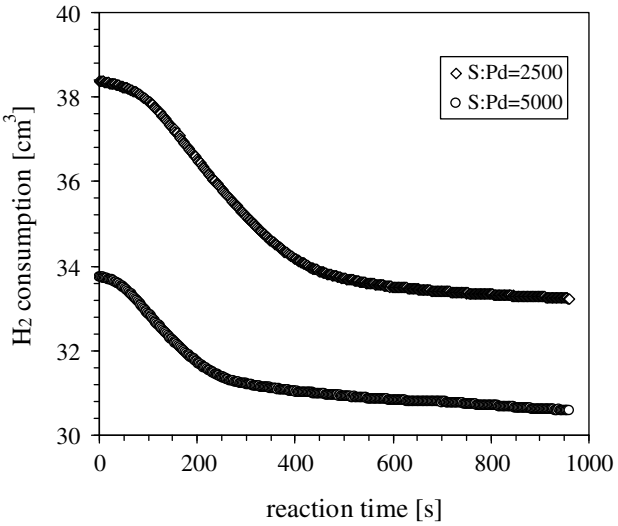

Fig. 8 – Hydrogenation of 4-octyne over Pd–GO $m = 5 \times 10^{-5}$ g, $T = 298$ K, $p = 10^5$ Pa, S:Pd = 10,000.

It may be observed in Table 1 that the Pd–GO sample exhibited pronounced catalytic activities and high (Z)-alkene stereoselectivities for both reactants. The initial rates and the turnover frequencies proved to be substantially high values, which displayed no appreciable variation with the S:Pd ratio (except for the application of S:Pd = 10,000 for 3-hexyne, which resulted in a decreased activity). When the S:Pd ratio was increased, the reaction time required for complete

Table 1 – Catalytic hydrogenations of internal alkynes over Pd–GO

Reactant[a]	S:Pd	Conversion (%)	$S_{(Z)}$ (%)	$S_{(E)}$ (%)	S_{alkane} (%)	R (cm^3 H_2 min^{-1} g Pd^{-1})	TOF (s^{-1})
3-Hexyne[b]	2500	99.7	98.41	1.37	0.22	89,326	25.9
3-Hexyne[c]	5000	99.4	98.22	1.39	0.30	103,618	30.0
3-Hexyne[d]	10,000	78.1	97.40	2.29	0.31	64,315	18.7
4-Octyne[c]	2500	100	93.86	0.41	5.73	92,899	27.0
4-Octyne[d]	5000	66.2	93.14	0.29	6.57	125,056	36.3

a $m = 5 \times 10^{-5}$ g, $T = 298$ K, $p = 10^5$ Pa, solvent: 1 cm^3 of toluene.
b $t = 8$ min.
c $t = 15$ min.
d $t = 30$ min.

Table 2 – Hydrogenations of internal alkynes over supported Pd catalysts

Catalyst[a]	Reactant	$S_{(Z)}$[b] (%)	$S_{(E)}$[b] (%)	$S_{(alkane)}$[b] (%)	R (cm^3 H_2 min^{-1} g Pd^{-1})	TOF (s^{-1})
Pd/C	3-hexyne	98.04	1.39	0.57	34,796	14.8
Pd/graphimet	3-hexyne	98.19	1.47	0.34	42,428	12.3
Pd/C	4-octyne	94.12	0.39	5.49	44,336	18.9
Pd/graphimet	4-octyne	95.76	0.26	3.98	25,249	7.3

a $m = 5 \times 10^{-5}$ g, $T = 298$ K, $p = 10^5$ Pa, S:Pd = 2500, solvent: 1 cm^3 of toluene.
b Conversion: 40%.

conversion was found to be longer. The Pd–GO sample proved to be a particularly efficient catalyst for the transformation of 3-hexyne at S:Pd = 2500, for which hydrogenation was completed in 8 min and the stereoselectivity of (*Z*)-alkene formation was 98.41%. It may be readily seen that the catalyst exhibited marked (*Z*)-alkene stereoselectivities for both reactants, which surpassed 97% and 93% for 3-hexyne and 4-octyne, respectively. An increase in the S:Pd ratio was found to decrease the (*Z*) stereoselectivity, but only to a minor extent. In view of the above findings, it may be ascertained that Pd–GO was a highly active and stereoselective catalyst.

As compared with the formation of the *Z*-alkene stereoisomers, the formation of by-products was found to be negligible. For the transformation of 3-hexyne, a small amount of (*E*)-alkene was detected in the product mixture, whereas overhydrogenation was insignificant. In contrast, for the hydrogenation of 4-octyne, overhydrogenation predominated over the formation of the (*E*)-alkene stereoisomer. The enhanced selectivity of alkane formation, observed for 4-octyne, may be related to the pronounced decrease of the hydrogenation rate, displayed in Fig. 6. As related to the layered structure of the GO host and the increased molecular dimension of 4-octyne, the reaction rate is assumed to be controlled by mass transport limitations, which tend to restrict desorption of the (*Z*)-alkene molecules from the interlamellar active sites and thereby favour their readsorption, leading to overhydrogenation. The improved catalytic performance observed for 3-hexyne may be attributed to the relatively small size of this reactant, which ensures ready access to the interlamellar active sites of the catalyst [31].

The results obtained for the catalytic investigations of Pd/C and Pd/graphimet under the same conditions are listed in Table 2. For a meaningful comparison, the product selectivities were determined at the same conversion level of 40%.

The product selectivities obtained for the supported catalysts were very similar and of the same order as those determined for Pd/GO at S:Pd = 2500 (see Table 1). The latter values, however, were obtained at complete conversions. At a conversion level of 40%, the (*Z*)-alkene stereoselectivities for the reactions of 3-hexyne and 4-octyne over Pd/GO were found to be somewhat higher: 98.8% and 94.9%, respectively. This implies that Pd/GO was the most stereoselective catalyst of all the samples for 3-hexyne hydrogenation, whereas for the reaction of 4-octyne, no appreciable difference could be pointed out. On the other hand, a pronounced difference was observed between the samples in terms of the catalytic activity. As compared with the supported catalysts, Pd/GO displayed a much higher activity, as revealed by the values of both the reaction rates and the turnover frequencies. It may therefore be established that Pd/GO was a more efficient catalyst for alkyne hydrogenation than the supported Pd catalysts. The marked catalytic activity of Pd/GO may be attributed in part to its low Pd content and also to the relatively small size of the Pd particles, which ensures an enhanced number of active sites available for the reactant molecules.

4. Conclusions

Owing to its marked cation exchange capacity, swelling and intercalation ability, graphite oxide was utilized as a host material for the generation of Pd nanoparticles. A low-loaded Pd–GO sample was synthesized by immobilization of the precursor $Pd(NH_3)_4(NO_3)_2$ in GO via ion exchange, followed by reduction in H_2 stream. Structural characterization gave evidence that ion exchange resulted in the formation of $Pd(NH_3)_4^{2+}$ cations intercalated in GO and the reduced Pd nanoparticles were situated both on the external surface and in the interlamellar space of the GO host. The mean crystallite diameter, determined for the external particles, was

3.54 nm. The catalytic performance of the Pd–GO sample was investigated in the liquid-phase hydrogenations of 3-hexyne and 4-octyne. For both reactants, high turnover frequencies (18–36 s^{-1}) were determined, revealing a pronounced catalytic activity, which displayed no systematic variation with the S:Pd ratio. The catalytic activity of Pd/GO considerably surpassed those of supported Pd catalysts, whereas the stereoselectivity of (*Z*)-alkene formation was of the same order. It is suggested that intercalated Pd particles participate in the catalytic reactions as active sites. Such particles appear to be readily accessible for 3-hexyne, whereas for 4-octyne, the hydrogenation rate tends to be controlled by mass transport limitations.

Acknowledgments

Financial support obtained from the Hungarian Academy of Sciences (OTKA Grant K 68152) and the Hungarian Science and Technology Foundation (Grant OMFB-00010/2008) is gratefully acknowledged. We would like to express our special thanks to Dr. Ottó Berkesi, for his valuable assistance with the IR measurements.

REFERENCES

[1] Beckett RJ, Croft RC. The structure of graphite oxide. J Phys Chem 1952;56(8):929–34.
[2] Stankovich S, Piner RD, Nguyen ST, Ruoff RS. Synthesis and exfoliation of isocyanate-treated graphene oxide nanoplatelets. Carbon 2006;44:3342–7.
[3] Nakajima T, Matsuo Y. Formation process and structure of graphite oxide. Carbon 1994;32:469–75.
[4] Szabó T, Tombácz E, Illés E, Dékány I. Enhanced acidity and pH-dependent surface charge characterization of successively oxidized graphite oxides. Carbon 2006;44:537–45.
[5] Liu Z, Wang ZM, Yang X, Ooi K. Intercalation of organic ammonium ions into layered graphite oxide. Langmuir 2002;18:4926–32.
[6] Boehm HP, Clauss A, Fischer G, Hofmann U. Surface properties of extremely thin graphite lamellae. In: Extended abstracts, 5th conference on carbon. Pennsylvania (Pennsylvania, USA): American Carbon Committee, Pergamon Press, New York; 1962. p. 73–80.
[7] Bourlinos AB, Gournis D, Petridis D, Szabó T, Szeri A, Dékány I. Graphite oxide: chemical reduction to graphite and surface modification with primary aliphatic amines and amino acids. Langmuir 2003;19:6050–5.
[8] Dékány I, Krüger-Grasser R, Weiss A. Selective liquid sorption properties of hydrophobized graphite oxide nanostructures. Colloid Polym Sci 1998;276:570–6.
[9] Lerf A, He H, Forster M, Klinowski J. Structure of graphite oxide revisited. J Phys Chem B 1998;102:4477–82.
[10] Hontoria-Lucas C, Lopez-Peinado AJ, Lopez-Gonzalez JD, Rojas-Cervantes ML, Martín-Aranda RM. Study of oxygen-containing groups in a series of graphite oxides. Physical and chemical characterization. Carbon 1995;33:1585–92.
[11] Lerf A, Buchsteiner A, Pieper J, Schöttl S, Dékány I, Szabó T, et al. Hydration behaviour and dynamics of water molecules in graphite oxide. J Phys Chem Solids 2006;67:1106–10.
[12] Stankovich S, Dikin DA, Dommett GHB, Kohlhaas KM, Zimney EJ, Stach EA, et al. Graphene-based composite materials. Nature 2006;442:282–6.
[13] Kotov NA, Dékány I, Fendler JH. Ultrathin garphite oxide-polyelectrolyte composites prepared by self-assembly: transition between conductive and non-conductive states. Adv Mater 1996;8:637–41.
[14] Matsuo Y, Niwa T, Sugie Y. Preparation and characterization of cationic surfactant-intercalated graphite oxide. Carbon 1999;37:897–901.
[15] Matsuo, Hatase K, Sugie Y. Monomer emission from pyrene adsorbed in surfactant-intercalated graphite oxide. Chem Commun 1999:43–4.
[16] Brodie BC. Sur le poids atomique du graphite. Ann Chim Phys 1860;59:466–72.
[17] Kovtyukhova NI, Karpenko GA. The interaction of Cu(+2) amine ions with graphite oxide. Mater Sci Forum 1992;91–93:219–23.
[18] Kovtyukhova N, Buzaneva E, Senkevich A. Ultrathin supported graphite oxide and carbon films. Carbon 1998;36:549–54.
[19] Mastalir Á, Király Z. Pd nanoparticles in hydrotalcite: mild and highly selective catalysts for alkyne semihydrogenation. J Catal 2003;220:372–81.
[20] Aben PC. Palladium areas in supported catalysts. Determination of palladium surface areas in supported catalysts by means of hydrogen chemisorption. J Catal 1968;10:224–9.
[21] Mastalir Á, Notheisz F, Bartók M, Haraszti T, Király Z, Dékány I. Structural properties and catalytic activity of Pd–graphimet. Appl Catal A 1996;144:237–48.
[22] Szöllősi Gy, Mastalir Á, Király Z, Dékány I. Preparation of Pt nanoparticles in the presence of a chiral modifier. J Mater Chem 2005;15:2464–9.
[23] Bailey S, King F. Catalytic hydrogenation and dehydrogenation. In: Sheldon RA, van Bekkum H, editors. Fine chemicals through heterogeneous catalysis. New York: Wiley; 2001. p. 351–62.
[24] Bond GC, Wells PB. The mechanism of the hydrogenation of unsaturated hydrocarbons on transition metal catalysts. Adv Catal 1964;15:91–226.
[25] Bond GC, Wells PB. The hydrogenation of acetylene II. The reaction of acetylene with hydrogen catalyzed by alumina-supported palladium. J Catal 1965;5:65–73.
[26] Gutmann H, Lindlar H. Partial catalytic hydrogenation of acetylenes. In: Viehe HG, editor. Chemistry of acetylenes. New York: Dekker; 1969. p. 355–64.
[27] Molnár Á, Sárkány A, Varga M. Hydrogenation of carbon–carbon multiple bonds: chemo-, regio- and stereo-selectivity. J Mol Catal A Chem 2001;173:185–221.
[28] Panpranot J, Pattamakomsan K, Goodwin Jr JG, Prasertham P. A comparative study of Pd/SiO_2 and Pd/MCM-41 catalysts in liquid-phase hydrogenation. Catal Commun 2004;5:583–90.
[29] Carturan G, Facchin G, Cocco G, Enzo S, Navazio G. Influence of metal dispersion on selectivity and kinetics of phenylacetylene hydrogenation catalyzed by supported palladium. J Catal 1982;76:405–17.
[30] Mastalir Á, Király Z, Berger F. Comparative study of size-quantized Pd–montmorillonite catalysts in liquid-phase semihydrogenations of alkynes. Appl Catal A Gen 2004;269:161–8.
[31] Mastalir Á, Rác B, Király Z, Molnár Á. In situ generation of Pd nanoparticles in MCM-41 and catalytic applications in liquid-phase alkyne hydrogenations. J Mol Catal A Chem 2007;264:170–8.